Materials Research Bulletin 149 (2022) 111725

Contents lists available at ScienceDirect

Materials Research Bulletin

journal homepage: www.elsevier.com/locate/matresbu

Cr^{3+}-doped broadband near infrared diopside phosphor for NIR pc-LED

Limin Fang [a,b], Zhendong Hao [*,a], Liangliang Zhang [a], Hao Wu [a], Huajun Wu [a], Guohui Pan [a], Jiahua Zhang [*,a,b]

[a] State Key Laboratory of Luminescence and Applications, Changchun Institute of Optics, Fine Mechanics and Physics, Chinese Academy of Sciences, Changchun 130033, China

[b] Center of Materials Science and Optoelectronic Engineering, University of Chinese Academy of Sciences, Beijing 100049, China

ARTICLE INFO

Keywords:
A. inorganic compounds
B. luminescence
D. phosphors

ABSTRACT

Broadband Near-infrared phosphors have attracted great attention for its potential applications in pc-LED as a novel light source for substance measurements based on NIR spectroscopy. Here, $CaMgSi_2O_6:xCr^{3+}$ diopside phosphor were prepared by high temperature solid-state reaction. The Cr^{3+}emission band undergoes a red-shift from 772 nm to 822 nm followed with band broadening from 132 nm to 197 nm with the increase of x from 0.25% to 6%. Highly thermal stability with the quenching temperature as high as 355 °C for 1% and 236 °C for 4% Cr^{3+} concentrations are observed. NIR pc-LEDs were fabricated and high NIR output power of 42.04 mW for the bandwidth of 150 nm and 23.73 mW for a more broaden bandwidth of 187 nm are achieved at 100 mA drive current, respectively. Our results suggest that $CaMgSi_2O_6:Cr^{3+}$phosphors have great potential for applications in broadband NIR pc-LED applications.

Abbreviations

NIR	Near-infrared
pc-LED	phosphor converted light emitting diode
PL	Photoluminescence
SLD	superluminescent diode
DOT	diffuse optical tomography
FWHM	full width at half maximum
CFSE	crystal field stabilization energy
QE	quantum efficiency
RT	room temperature.

1. Introduction

Near infrared phosphor converted light emitting diode (NIR pc-LED) is a new type of solid-state NIR light source for substance measurements based on NIR spectroscopy. Compared with the traditional light source such as tungsten halogen lamp and superluminescent diode (SLD), the NIR pc-LED has the advantages of high efficiency, compact size, low cost, good durability and low working voltage. NIR pc-LED light source is a key technology for miniaturization and integration of NIR spectrometer. NIR spectroscopy technology has widespread applications in agriculture, food, pharmacy, medicine and other fields [1,2]. Because near-infrared light can penetrate the scalp layer, skull layer to cerebral cortex, NIR pc-LED light source can be applied to the field of neuroscience by diffuse optical tomography (DOT) bio-imaging Technology. DOT technology is used to monitor local neural activity by monitoring the changes of cerebral blood flow [3,4]. Thereby, to develop efficient NIR phosphors with the emission band as broad as possible is the key segment for broadband NIR pc-LED light sources.

Transition metal Cr^{3+} is the commonly selected luminescent center for broadband NIR emission for blue excitation when situated in weak and intermediate octahedral crystal field. In recent years, many Cr^{3+} doped broadband NIR phosphors have been reported. Most of them have a full width at half maximum (FWHM) less than 150 nm [5–13], A few Cr^{3+} activated phosphors show a super broad NIR emission band, but their photoluminescence (PL) yields are not high. $La_3Ga_5GeO_{14}:Cr^{3+}$ garnet phosphor exhibits a NIR emission band with a FWHM of 330 nm and the fabricated pc-LED offered NIR output of 18.2 mW at 350 mA drive current [14]; $Mg_3Ga_2GeO_8:Cr^{3+}$ phosphor with the FWHM of 244 nm, and fabricated pc-LED had a NIR output of 6.143 mW at 60 mA drive current after applied to pc-LED [15]; Yao et al. developed $LiScP_2O_7:Cr^{3+}$ with FWHM of ~170 nm. The fabricated pc-LED had a NIR output of 19 mW at 100 mA drive current [16]. Codoping Cr^{3+} and Yb^{3+} is an effective strategy for achieving super broad emission band with guaranteed efficiency [16–19]. For the light source of spectral analysis

* Corresponding authors.
E-mail addresses: haozd@ciomp.an.cn (Z. Hao), zhangjh@ciomp.an.cn (J. Zhang).

https://doi.org/10.1016/j.materresbull.2021.111725
Received 15 October 2021; Received in revised form 29 December 2021; Accepted 30 December 2021
Available online 2 January 2022

system, the emission spectra should be as flat as possibles. However, in this kind of codoped phosphors, Yb^{3+} ions introduce sharp line emission into the PL spectra. Therefore, it is of great theoretical and practical value to actively explore new broadband near-infrared luminescent materials.

Diopside ($CaMgSi_2O_6$) is one of the main crystal phases in common silicate materials and belongs to pyroxene group. $CaMgSi_2O_6:Eu^{2+}$ is well known as a blue phosphor for plasma display panel [20,21], where Eu^{2+} ion occupy Ca^{2+} sites of Diopside. There are some reports on Cr^{3+} doped $CaMgSi_2O_6$ Crystal for tunable and ultrashort laser [22–24]. In pc-LED technology, powder luminescent materials need to be mixed with adhesive and then coated on bule LED chips, therefore NIR phosphor is more convenient and cost-effective that these crystals.

In this work, blue light excitable Cr^{3+}-activated $CaMgSi_2O_6$ broadband NIR phosphors were synthesized by high temperature solid-state reaction. The FWHM of the NIR emission band broadens from 132 nm further to 197 nm with the increase of Cr^{3+} concentration from 0.25% to 6%. Temperature dependent emission intensity was investigated. The NIR pc-LEDs were fabricated by using $CaMgSi_2O_6$: 1%Cr^{3+} or $CaMgSi_2O_6$: 4%Cr^{3+} phosphors based on blue LED chips. The performance of the NIR pc-LEDs were evaluated. The NIR output of 42.04 mW with the bandwidth of 150 nm and 23.73 mW with the bandwidth of 187 nm are achieved at 100 mA drive current, respectively.

2. Experimental

2.1. Materials and preparation

Powder samples with compositions of $CaMg_{1-x}Si_2O_6:xCr^{3+}$ (abbreviated to $CaMgSi_2O_6:xCr^{3+}$ hereafter) were prepared by conventional high-temperature solid-state reaction method. The starting materials of $CaCO_3$(99%), MgO(98%), SiO_2(99%) and Cr_2O_3(99.95%) were weighed according to the given stoichiometric ratio. In addition, 0.06 mole ratio of NaCl(99.8%) was added as both flux and charge compensator. Then these starting materials were homogeneously mixed and ground in an agate mortar for 45 min. After that, the mixture was transferred into a corundum crucible and put into a muffle furnace sintered in air. The temperature was first maintained at 900 °C for 1 hour and then raised to 1250 °C for 3 h. At last, the furnace was cooled down to room temperature and these samples were ground into fine powders, washed with acetic acid solution, filtered and dried for subsequent characterization.

2.2. Characterizations

The crystal structure of these as-prepared samples was examined by X-ray diffraction (XRD) using a D8 Focus diffractometer (Bruker, Germany) with Cu Kα radiation source. The operation voltage and current was set at 40 kV and 30 mA, respectively. Room-temperature photoluminescence excitation spectra (excitation spectra) and room-temperature photoluminescence intensity were recorded using a FLS920 fluorescence spectrophotometer (Vis detector 200–900 nm, NIR detector 850–1700 nm, Edinburgh Instrument, UK) equipped with a 150 W Xe lamp. Room-temperature photoluminescence spectra (emission spectra) were recorded using FLS920 fluorescence spectrophotometer and a HAAS2000 photoelectric measuring system (350–1100 nm, EVERFINE, Cina) equipped with 455 nm laser diode. And both detectors are calibrated with the same HL-3 VIS-NIR light source (Ocean Optics, USA). Diffuse reflection spectra were recorded using a UV-3600 plus UV–Vis-NIR spectrometer (Shimadzu, Japan) equipped with an integrating sphere. $BaSO_4$ powder was using for standard reference. The fluorescence decay curves of the as-prepared samples were using a pulsed laser from an optical parametric oscillator as the excitation source, the transient fluorescence was obtained by a TRIAX 550 spectrometer, and the electric signal was measured by a Tektronix digital oscilloscope. The temperature dependent properties were measured using a 455 nm laser diode as the excitation source, a THMS600E cooling-heating platform (77–873 K, Linkam Scientific Instruments, UK) and a QEPro micro fiber spectrometer. The quantum efficiency was recorded using the HAAS 2000 photoelectric measuring system equipped with an integrating sphere, and a 660 nm laser diode power by precision DC stabilized current power supply of HAAS 2000 as excitation light source. The photoelectric properties of the pc-LEDs were measured using the HAAS 2000 photoelectric measuring system equipped with an integrating sphere.

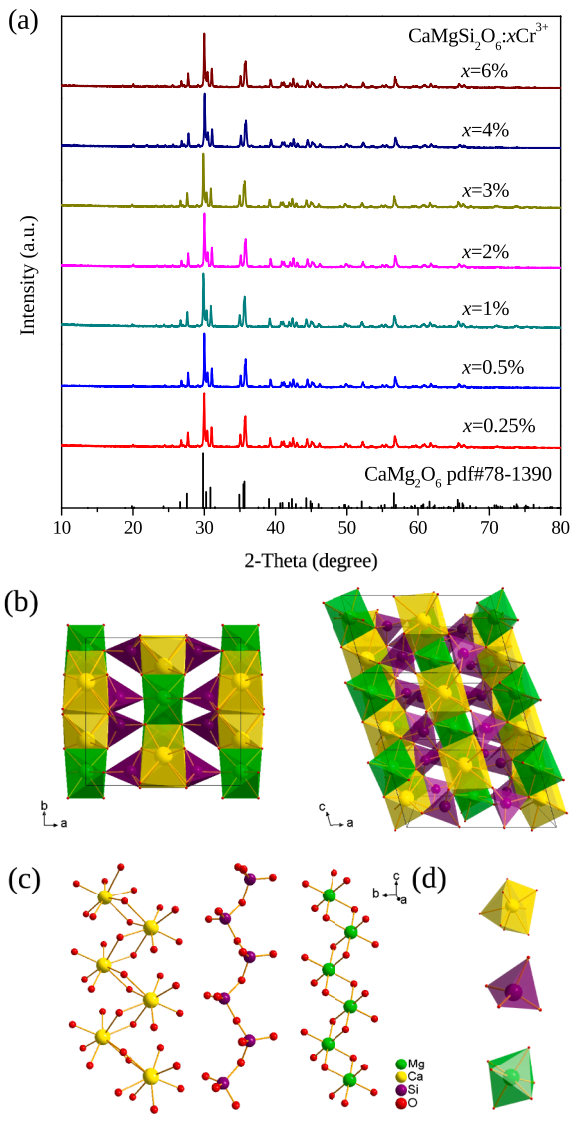

Fig. 1. Structural characterization and analysis. (a)XRD patterns of $CaMgSi_2O_6$: x Cr^{3+}; (b) structural model of $CaMgSi_2O_6$ diopside 1 × 1 × 3 cells. (c) Schematic diagram of CaO_8 dodecahedral single chain, SiO4 tetrahedral single chain and MgO_6 octahedral single chain; (d) Schematic diagram of CaO_8 dodecahedral site, MgO_6 octahedral site and SiO_4 tetrahedral site.

3. Results and discussion

3.1. Phase identification

The XRD patterns of $CaMgSi_2O_6:x:Cr^{3+}$broadband near-infrared phosphors are shown in **Fig. 1(a)**. It can be seen that the diffraction peaks can be well assigned to the standard data of $CaMgSi_2O_6$ diopside (PDF #78–1390), indicating that the introduction of Cr^{3+} ions had no significant effect on the structure of the phosphors. The crystal structure

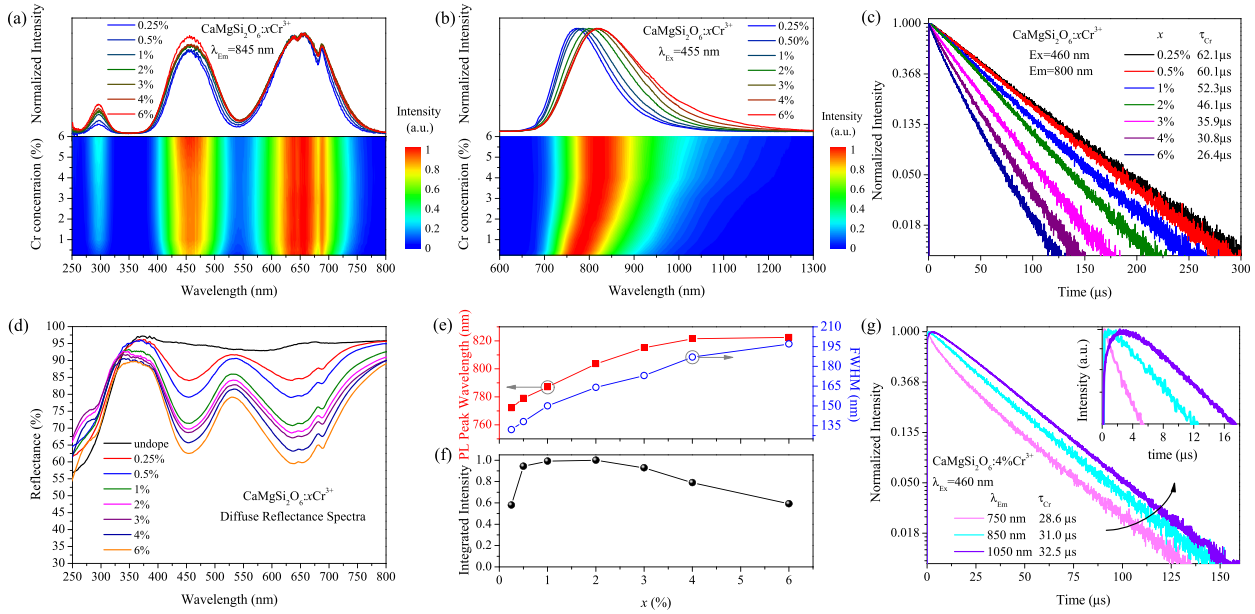

Fig. 2. Normalized excitation spectra (a) and emission spectra (b) of $CaMgSi_2O_6$:xCr^{3+}; (c) fluorescence decay of $CaMgSi_2O_6$:xCr^{3+} monitored at 800 nm upon 460 nm excitation; (d) Diffuse reflectance spectra of $CaMgSi_2O_6$:xCr^{3+}; x dependence of (e) emission peak wavelength, emission width and (f) integrated intensity of NIR emission under 455 nm excitation; (g) fluorescence decay of $CaMgSi_2O_6$:4%Cr^{3+} monitored at different wavelengths upon 460 nm excitation.

of $CaMgSi_2O_6$ diopside is based on the space group C2/c (No. 15), belonging to the monoclinic system. **Fig. 1(b)** displays the structure model of $CaMgSi_2O_6$ diopside 1 × 1 × 3 cell. The $CaMgSi_2O_6$ structure consists of MgO_6 octahedral single chains, SiO_4 tetrahedral single chains and CaO_8 dodecahedral single chains arranged along the c axis [25,26]. As shown in **Fig. 1(c)**, MgO_6 octahedral single chains and CaO_8 dodecahedral single chains are connected by sharing edges, SiO_4 tetrahedral single chains are connected by sharing vertexes.

As the ionic radius of Ca^{2+} (CN = 8), Mg^{2+} (CN = 6) and Si^{4+} (CN = 4) are 1.12 Å, 0.72 Å and 0.26 Å, respectively. The ionic radius of Cr^{4+} (CN = 4), Cr^{3+} (CN = 6) are 0.41 Å, 0.615 Å, respectively [27], and the ionic radius of Na^+ (CN =8) is 1.18 Å, as shown in **Fig. S1**. The Cr^{3+} ion has higher crystal field stabilization energy (CFSE) [28,29] . Therefore, it is easier for chromium to enter the octahedral sites of Mg^{2+} ions in the form of trivalent ions. The radius of Na^+ is close to the radius of Ca^{2+}, we believe that Na^+ ions enter Ca^{2+} sites and form charge compensation relationship with Cr^{3+} ions: $Na^+ + Cr^{3+} \rightarrow Ca^{2+} + Mg^{2+}$. On the other hand, the melting point of NaCl is 801℃, so NaCl should act as both flux and charge compensator.

3.2. Photoluminescence properties

As shown in **Fig. 2(a)**, with the increase of Cr^{3+} doping concentration, excitation spectra of $CaMgSi_2O_6$:xCr^{3+} has no obvious change. These excitation spectra monitored at 845 nm contain three excitation bands originate from spin-allowed transitions of Cr^{3+} ions: they are excitation bands around in the ultraviolet region correspond to $^4A_2 \rightarrow {}^4T_1(^4P)$ transition, blue region correspond to $^4A_2 \rightarrow {}^4T_1$ transition and red region correspond to $^4A_2 \rightarrow {}^4T_2$ transition of Cr^{3+} ions, respectively. In addition, These excitation also contain excitation peaks originate from spin-forbidden transitions of Cr^{3+} ions: they are excitation peaks around 638 nm and 655 nm correspond to $^4A_2 \rightarrow {}^2T_1$ transition, 688 nm correspond to $^4A_2 \rightarrow {}^2E$ transition [30], respectively. The diffuse reflectance spectra of $CaMgSi_2O_6$:xCr^{3+}were measured, the absorption of $CaMgSi_2O_6$:xCr^{3+} samples increased with the increase of Cr doping concentration and the diffuse reflectance spectrum of $CaMgSi_2O_6$:Cr^{3+}phosphors correspond to the excitation spectrum.

Normalized emission spectra of $CaMgSi_2O_6$:xCr^{3+} excited by 455 nm blue light are shown in **Fig. 2(b)**. It can be seen that with the increase of Cr^{3+} doping concentration x from 0. 25% to 6%, the emission band shows a red-shift from 772 nm to 822 nm and a broadening from 132 nm to 197 nm. This is an important characteristic for $CaMgSi_2O_6$:Cr^{3+}phosphors in near infrared spectroscopy application. The emission integral intensity of $CaMgSi_2O_6$:xCr^{3+} reaches the maximum when Cr^{3+} doping concentration is 2%. The fluorescence decay curve of $CaMgSi_2O_6$:xCr^{3+} monitored at 800 nm after pulse excitation at 460 nm was recorded and is shown in **Fig. 2(c)**. It can be seen that with the increase of Cr^{3+} doping concentration, the fluorescence lifetimes of Cr^{3+} are shortened from 62.1 μs to 26.4 μs, due to the increased of nonradiative transition.

There may be multiple reasons for such the significant broadening and red-shift of the emission band. Firstly, as shown in **Fig. 2(g)**, for the high Cr doped sample $CaMgSi_2O_6$:4%Cr^{3+}, as the monitoring wavelength moves towards the long wave direction, the fluorescence lifetime increases followed with appearance of a rising edge with tuning the monitored wavelengths towards the longer wavelengths, which means that there is energy transfer from the short wave position to the long wave position. There are two possible sources of this energy transfer: one is increased energy transfer from high energy Cr^{3+} ions to low energy Cr^{3+} ions in inhomogeneous environment of the activator ions [31,32]. Even in the same sample, the microenvironment around different Cr^{3+} ions is different, resulting in that the emission energy of some Cr^{3+} ions is lower than that of other Cr^{3+} ions. With the increase of Cr^{3+} ion doping concentration, the energy transfer from high-energy Cr^{3+} to low-energy Cr^{3+} ions can occur and increase, resulting in significant broadening and red shift of the emission band. Another possible source is the existence of the second lattice site that emits at longer wavelength. In $CaMgSi_2O_6$:Cr crystal, Two emission peaks near 800 nm and 1000 nm can be observed in $CaMgSi_2O_6$:Cr crystal. The emission peak around 800 nm comes from the Cr^{3+} emission of Mg octahedral lattice, and the emission peak near 1000 nm corresponds to the Ca vacancies or the second lattice site introduced by Ca and Mg deviating from the stoichiometric ratio [22–24]. In our $CaMgSi_2O_6$:Cr phosphor, no second sub peak was observed near 1000 nm, because we introduced Na^+ as charge compensator. But there may still be a small number of second lattice remaining and participating in the above energy transfer process and contribute to the red shift and broadening of the emission band.

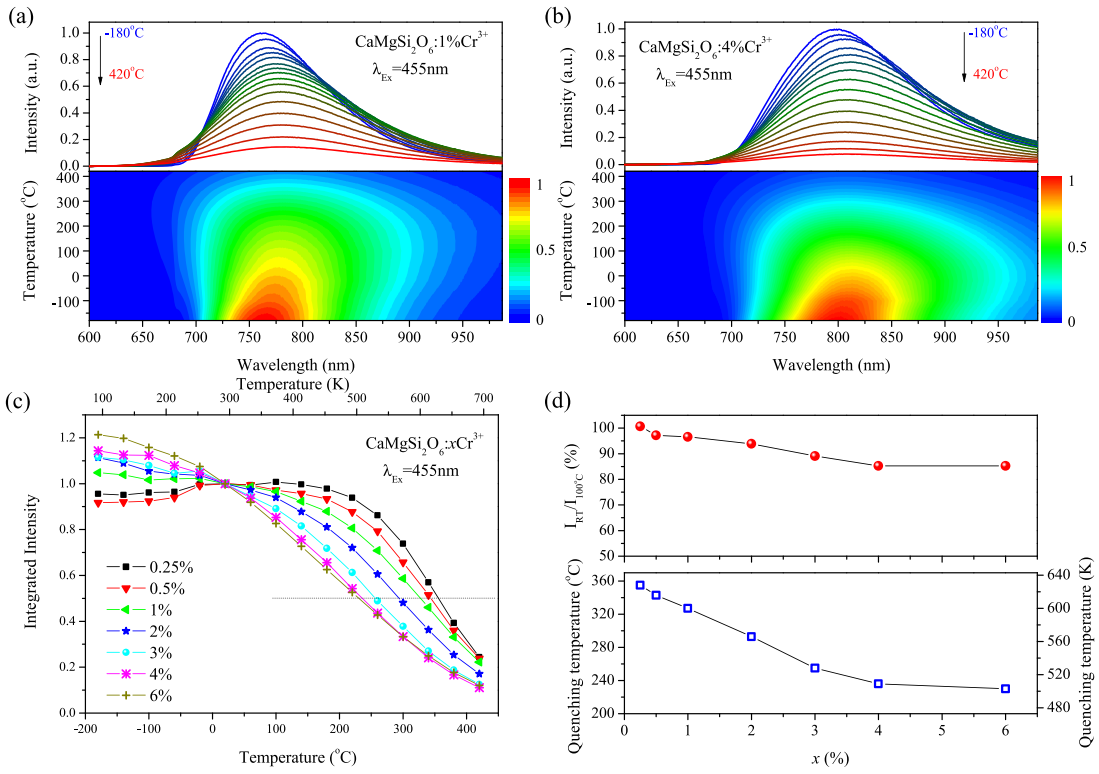

Fig. 3. Temperature-dependent emission spectra of (a) $CaMgSi_2O_6$:1%Cr^{3+} and (b) $CaMgSi_2O_6$:4%Cr^{3+}; (c) temperature-dependent integrated emission intensities for $CaMgSi_2O_6$:xCr^{3+}; (d) ratio of emission integrated intensity of phosphor at 100 ℃ to emission integrated intensity at room temperature; (e) quenching temperature of $CaMgSi_2O_6$:xCr^{3+}.

3.3. *Temperature dependent emission spectra*

To investigate the thermal quenching behavior of the NIR phosphors, temperature dependent emission spectra measurement was performed. Temperature-dependent emission spectra of $CaMgSi_2O_6$:1%Cr^{3+} and $CaMgSi_2O_6$:4%Cr^{3+} are shown in **Fig. 3(a)(b).** For low Cr doped

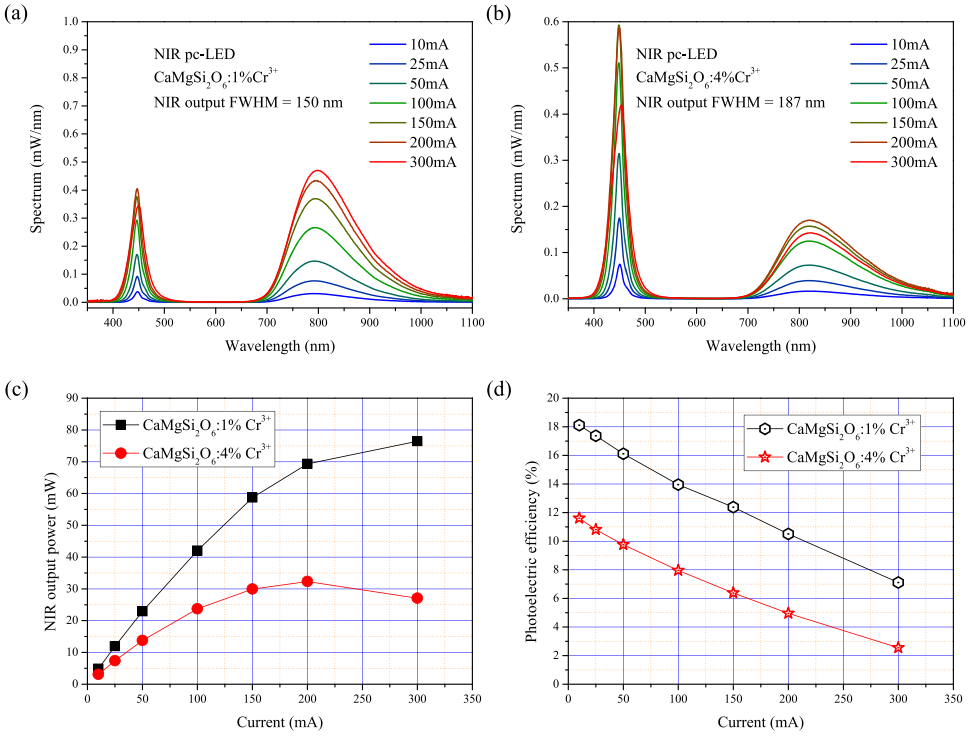

Fig. 4. Emission spectra of the NIR pc-LEDs fabricated by (a)$CaMgSi_2O_6$:1%Cr^{3+}, (b)$CaMgSi_2O_6$:4% Cr^{3+} (c) NIR output power (650 nm-1100 nm) of the NIR pc-LEDs fabricated by $CaMgSi_2O_6$: Cr^{3+}; (d) Photoelectric efficiency of the NIR pc-LEDs fabricated by $CaMgSi_2O_6$: Cr^{3+}.

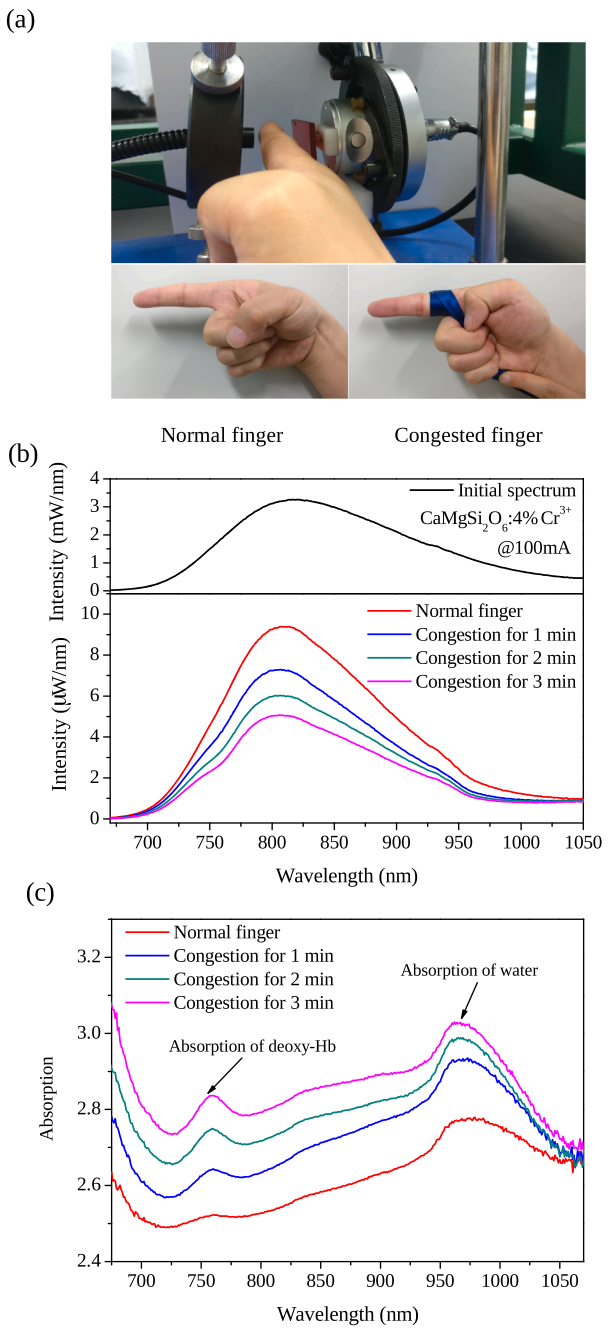

Fig. 5. (a) Photographs of the experimental setup, normal finger and congested finger;(b) Spectra of NIR light after penetrating human finger; (c) Calculated absorption spectra of human finger in different condition.

samples, the emission spectra broadening and red-shift obviously and continuously with the increase of the temperature. For high Cr doped samples, the spectral broadening and red-shift stop when it reaches a certain temperature. Fig. 3**(c)** displays the integrated emission intensities in $CaMgSi_2O_6$:xCr^{3+} as a function of temperature. Generally speaking, with the increase of Cr doping concentration, the thermal quenching behavior of the NIR phosphors are more serious. This phenomenon also occurs in YAG:Ce, which is explained as thermally activated concentration quenching [33]. As shown in Fig. 3**(d)**, 96% and 85% of the emission integrated intensity at room temperature can be retain at 373 K(100 °C) for samples doped with 1% and 4% Cr^{3+} respectively. The thermal quenching temperature is defined as the temperature at which the emission integrated intensity is reduced by half than that at room temperature. As shown in Fig. 3**(e)** The thermal quenching temperature reaches 600 K (327 °C) for 1% Cr doping samples, and 509 K (236 °C) for 4% Cr doping samples. As listed in Table 1, $CaMgSi_2O_6$:1%Cr^{3+} are among the highest thermal stability of Cr^{3+}doped NIR phosphors, while $CaMgSi_2O_6$:4%Cr^{3+} still maintained high thermal stability.

3.4. Quantum efficiency and application to NIR pc-LED

Considering the $CaMgSi_2O_6$:1%Cr^{3+} still has high luminescence intensity and quenching temperature of more than 300 ℃ on the premise of ensuring the 150 nm bandwidth, and $CaMgSi_2O_6$:4%Cr^3 has a super broadband emission of 187 nm without losing to much luminescence intensity and thermal stability. So we chose these samples for further testing. The quantum efficiency (QE) of $CaMgSi_2O_6$:1%$Cr^{3+}$and $CaMgSi_2O_6$:4%Cr^{3+} were measured to characterize their luminescent efficiency, and the measured spectra are shown in **Fig. S6** Accordingly, the quantum efficiency upon 660 nm excitation is calculated as follows: $CaMgSi_2O_6$:1%Cr^{3+} have internal QE of 77.5% and external QE of 21.6%, and $CaMgSi_2O_6$:4%Cr^{3+} have internal QE of 45.9% and external QE of 16.5%.

NIR pc-LEDs were fabricated by combining the $CaMgSi_2O_6$:1%Cr^{3+}, $CaMgSi_2O_6$:4%Cr^{3+} phosphors with a 450 nm blue InGaN LED chip. The adhesive for package is epoxy resin. The mass ratio of epoxy resin to phosphor is 1:1. Fig. 4**(a)(b)** shows the emission spectra of the NIR pc-LEDs fabricated by selected phosphors. It can be seen that with the increase of the drive current, the spectral profile of the fabricated NIR pc-LED has no changes except for the increase in intensity. The NIR pc-LED fabricated using $CaMgSi_2O_6$:1% Cr^{3+} can offer photoelectric efficiency of 18.12% at 10 mA current and 13.95% at 100 mA current. The near-infrared light output is 42.04 mW at 100 mA current with the bandwidth of 150 nm. This result is the mainstream level for near-infrared phosphors with a bandwidth about 150 nm. The broadband NIR pc-LED fabricated using $CaMgSi_2O_6$:4% Cr^{3+}gives 11.60% photoelectric efficiency at 10 mA current and 7.96% at 100 mA current. The NIR output power of 23.73 mW with the bandwidth of 187 nm is achieved at 100 mA drive current. This is a very good result for Cr^{3+}singly doped NIR phosphors with the bandwidth wider than 180 nm.

In order to demonstrate the application prospect of $CaMgSi_2O_6$:Cr^{3+} phosphors in medical fields, spectra of NIR light emitted from NIR pc-LEDs fabricated by $CaMgSi_2O_6$:4% Cr^{3+} after penetrating human finger are measured. The experimental setup is shown in Fig. 5**(a)**, the optical fiber in the photo is connected to a HAAS 2000 photoelectric measuring system, and a 590 nm long-wavelength pass filter was used to block the blue light. We used a strap to bind around the finger to temporarily block venous blood flow back. Then three measurements were made every 1 min. The input current of NIR LED is 100 mA. Beer-Lambert law [36] is as follows:

$$I(\nu) = I_0(\nu)e^{-\alpha(\nu)L} \quad (1)$$

Table 1
Thermal stability of typical Cr^{3+}doped NIR phosphors.

Materials quenching temperature	quenching temperature(°C)	I_{RT}/ $I_{100\ °C}$(%)	Ref
$CaMgSi_2O_6$:1% Cr^{3+}	327	96.6	This Work
$CaMgSi_2O_6$:4% Cr^{3+}	236	85.3	This Work
$Ca_3Sc_2Si_3O_{12}$:Cr^{3+}	/	~100	[9]
$Ca_2LuHf_2Al_3O_{12}$:Cr^{3+}	~200	~85	[34]
$LiInSi_2O_6$:Cr^{3+}	~220	~88	[8]
$LiInGe_2O_6$:Cr^{3+}	~105	~52	[35]
$InBO_3$: Cr^{3+}	~150	70	[11]
$LiScP_2O_7$:0.06Cr^{3+}	~85	42	[16]
$LiScP_2O_7$:0.06Cr^{3+},0.05Yb^{3+}	~137	79	

Where $I_0(\nu)$ and $I(\nu)$ are the intensity of the light before and after absorption, respectively. $\alpha(\nu)$ is the absorption coefficient. L is the optical distance. The absorption spectra can be calculated by the following formula:

$$A(\nu) = -\log\left(\frac{I(\nu)}{I_0(\nu)}\right) = \frac{\alpha(\nu)L}{\ln(10)} \quad (2)$$

As shown in **Fig. 5(b)**, this setup with NIR pc-LED light source successfully picked up the spectral difference caused by finger congestion. The peaks at 760 nm and 965 nm in Fig. 5(c) correspond to the characteristic absorption of deoxy-Hb and water, respectively. The increased absorption of deoxy-Hb and water is consistent with the obstruction of blood flow back to the vein of the heart, resulting in venous congestion. ,
-

4. Conclusion

In general, Cr^{3+} doped $CaMgSi_2O_6$ broadband near-infrared diopside phosphors was prepared. Upon 450 nm excitation, the emission band shows a red-shift from 772 nm to 822 nm and a broadening from 132 nm to 197 nm with increasing *x* from 0.25% to 0.06%. Highly thermal stability with the quenching temperature as high as 355 °C for 1% and 236 °C for 4% Cr^{3+} concentrations are observed. NIR pc-LEDs were fabricated by using $CaMgSi_2O_6$: 1%Cr^{3+} or $CaMgSi_2O_6$: 4%Cr^{3+} phosphors based on blue LED chips. The NIR output of 42.04 mW with the bandwidth of 150 nm and 23.73 mW with the bandwidth of 187 nm are achieved at 100 mA drive current for 1%Cr^{3+} and 4%Cr^{3+} doped samples fabricated LED, respectively. These results suggest that $CaMgSi_2O_6$: Cr phosphors have great potential for applications in broadband NIR pc-LED.

Declaration of Competing Interest

The authors declare that they have no known competing financial interests or personal relationships that could have appeared to influence the work reported in this paper.

Acknowledgement

This work was partially supported by National Natural Science Foundation of China (Grant No. 11974346, 51772286, 52102192, 52072361, 12074373, 11904361, 11874055 and 12074374), Youth Innovation Promotion Association CAS No. 2020222, Key Research and Development Program of Jilin province (20200401050GX, 20200401004GX and 20210201024GX), Cooperation project between Jilin Province and Chinese Academy of Sciences (2020SYHZ0013). the Opening Project Key Laboratory of Transparent Opto-functional Inorganic Material, Chinese Academy of Sciences.

Supplementary materials

Supplementary material associated with this article can be found, in the online version, at doi:10.1016/j.materresbull.2021.111725.

References

[1] C. Pasquini, Near infrared spectroscopy: a mature analytical technique with new perspectives – A review, Anal. Chim. Acta. 1026 (2018) 8–36, https://doi.org/10.1016/j.aca.2018.04.004.
[2] B.M. Nicolaï, K. Beullens, E. Bobelyn, A. Peirs, W. Saeys, K.I. Theron, J. Lammertyn, Nondestructive measurement of fruit and vegetable quality by means of NIR spectroscopy: a review, Postharvest Bio. Tec. 46 (2007) 99–118, https://doi.org/10.1016/j.postharvbio.2007.06.024.
[3] F. Jobsis, Noninvasive, infrared monitoring of cerebral and myocardial oxygen sufficiency and circulatory parameters, Science 198 (1977) 1264–1267, https://doi.org/10.1126/science.929199.
[4] M. Ferrari, V. Quaresima, A brief review on the history of human functional near-infrared spectroscopy (fNIRS) development and fields of application, Neuroimage 63 (2012) 921–935, https://doi.org/10.1016/j.neuroimage.2012.03.049.
[5] Q. Shao, H. Ding, L. Yao, J. Xu, C. Liang, J. Jiang, Photoluminescence properties of a $ScBO_3$:cr^{3+} phosphor and its applications for broadband near-infrared LEDs, RSC. Adv. 8 (2018) 12035–12042, https://doi.org/10.1039/C8RA01084F.
[6] B. Malysa, A. Meijerink, T. Jüstel, Temperature dependent Cr^{3+} photoluminescence in garnets of the type $X_3Sc_2Ga_3O_{12}$ (X = Lu, Y, Gd, La), J. Lumin 202 (2018) 523–531, https://doi.org/10.1016/j.jlumin.2018.05.076.
[7] B. Malysa, A. Meijerink, T. Jüstel, Temperature dependent luminescence Cr^{3+}-doped $GdAl_3(BO_3)_4$ and $YAl_3(BO_3)_4$, J. Lumin. 171 (2016) 246–253, https://doi.org/10.1016/j.jlumin.2015.10.042.
[8] X. Xu, Q. Shao, L. Yao, Y. Dong, J. Jiang, Highly efficient and thermally stable Cr^{3+}-activated silicate phosphors for broadband near-infrared LED applications, Chem. Eng. J. 383 (2020), 123108, https://doi.org/10.1016/j.cej.2019.123108.
[9] Z. Jia, C. Yuan, Y. Liu, X.-J. Wang, P. Sun, L. Wang, H. Jiang, J. Jiang, Strategies to approach high performance in Cr^{3+}-doped phosphors for high-power NIR-LED light sources, Light Sci. Appl. 9 (2020) 86, https://doi.org/10.1038/s41377-020-0326-8.
[10] D. Yu, Y. Zhou, C. Ma, J.H. Melman, K.M. Baroudi, M. LaCapra, R.E. Riman, Non-Rare-Earth Na_3AlF_6 :cr^{3+} Phosphors for Far-Red Light-Emitting Diodes, ACS Appl. Electron. Mater. 1 (2019) 2325–2333, https://doi.org/10.1021/acsaelm.9b00527.
[11] Z. Sun, Q. Ning, W. Zhou, J. Luo, P. Chen, L. Zhou, Q. Pang, X. Zhang, Structural and spectroscopic investigation of an efficient and broadband NIR phosphor $InBO_3$: cr^{3+} and its application in NIR pc-LEDs, Ceram. Int. 47 (2021) 13598–13603, https://doi.org/10.1016/j.ceramint.2021.01.218.
[12] J. Lai, J. Qiu, Q. Wang, D. Zhou, Z. Long, Y. Yang, S. Hu, X. Li, J. Pi, J. Wang, Disentangling site occupancy, cation regulation, and oxidation state regulation of the broadband near infrared emission in a chromium-doped $SrGa_4O_7$ phosphor, Inorg. Chem. Front. 7 (2020) 2313–2321, https://doi.org/10.1039/D0QI00332H.
[13] S. Jiao, R. Pang, S. Wang, H. Wu, T. Tan, S. Zhang, L. Jiang, D. Li, C. Li, H. Zhang, Regulating chromium ions site occupancy and enhancing near-infrared luminescence properties of $Sr_2P_2O_7$:cr^{3+} phosphor through synthesizing under reduction atmosphere, Mater. Res. Bull. (2021), 111710, https://doi.org/10.1016/j.materresbull.2021.111710.
[14] D. Dai, Z. Wang, Z. Xing, X. Li, C. Liu, L. Zhang, Z. Yang, P. Li, Broad band emission near-infrared material $Mg_3Ga_2GeO_8$:cr^{3+}: substitution of Ga-In, structural modification, luminescence property and application for high efficiency LED, J. Alloy. Compd. 806 (2019) 926–938, https://doi.org/10.1016/j.jallcom.2019.07.166.
[15] V. Rajendran, M.-H. Fang, G.N.D. Guzman, T. Lesniewski, S. Mahlik, M. Grinberg, G. Leniec, S.M. Kaczmarek, Y.-S. Lin, K.-M. Lu, C.-M. Lin, H. Chang, S.-F. Hu, R.-S. Liu, Super Broadband Near-Infrared Phosphors with High Radiant Flux as Future Light Sources for Spectroscopy Applications, ACS Energy Lett 3 (2018) 2679–2684, https://doi.org/10.1021/acsenergylett.8b01643.
[16] L. Yao, Q. Shao, S. Han, C. Liang, J. He, J. Jiang, Enhancing Near-Infrared Photoluminescence Intensity and Spectral Properties in Yb^{3+} Codoped $LiScP_2O_7$: cr^{3+}, Chem. Mater. 32 (2020) 2430–2439, https://doi.org/10.1021/acs.chemmater.9b04934.
[17] Q. Shao, H. Ding, L. Yao, J. Xu, C. Liang, Z. Li, Y. Dong, J. Jiang, Broadband near-infrared light source derived from Cr^{3+} -doped phosphors and a blue LED chip, Opt. Lett. 43 (2018) 5251, https://doi.org/10.1364/OL.43.005251.
[18] S. He, L. Zhang, H. Wu, H. Wu, G. Pan, Z. Hao, X. Zhang, L. Zhang, H. Zhang, J. Zhang, Efficient Super Broadband NIR $Ca_2LuZr_2Al_3O_{12}$:cr^{3+},Yb^{3+} Garnet Phosphor for pc-LED Light Source toward NIR Spectroscopy Applications, Adv. Optical Mater. 8 (2020), 1901684, https://doi.org/10.1002/adom.201901684.
[19] D. Xu, Q. Zhang, X. Wu, W. Li, J. Meng, Synthesis, luminescence properties and energy transfer of Ca_2MgWO_6:cr^{3+},Yb^{3+} phosphors, Mater. Res. Bull. 110 (2019) 135–140, https://doi.org/10.1016/j.materresbull.2018.10.023.
[20] T. Kunimoto, H. Kobayashi, R. Yoshimatsu, S. Honda, E. Hata, S. Yamaguchi, K. Ohmi, Development of a new blue $CaMgSi_2O_6$:eu^{2+} phosphor for PDPs, J. Soc. Inf. Display. 13 (2005) 929, https://doi.org/10.1889/1.2137635.
[21] W.B. Im, J.H. Kang, D.C. Lee, S. Lee, D.Y. Jeon, Y.C. Kang, K.Y. Jung, Origin of PL intensity increase of $CaMgSi_2O_6$:eu^{2+} phosphor after baking process for PDPs application, Solid. State. Commun. 133 (2005) 197–201, https://doi.org/10.1016/j.ssc.2004.10.016.
[22] A.G. Avanesov, V.A. Lebedev, V.V. Zhorin, A.G. Okhrimchuk, A.V. Shestakov, Silicate crystals for infra-red lasers, J. Lumin. 72–74 (1997) 155–156, https://doi.org/10.1016/S0022-2313(96)00148-2.
[23] H. Mi, Y. Huang, Z. Lin, L. Zhang, G. Wang, Cr^{3+} -doped $CaMgSi_2O_6$ crystal: a promising tunable laser and ultrashort laser crystal, CrystEngComm 16 (2014) 763–765, https://doi.org/10.1039/C3CE41799A.
[24] Y. Huang, F. Yuan, L. Zhang, S. Sun, W. Qi, L. Zhoubin, Effects of Cr^{3+} ion concentration on the spectral characterization in Cr^{3+}:$ca_{0.93}Mg_{1.07}Si_2O_6$ crystals, J. Lumin. 211 (2019) 8–13, https://doi.org/10.1016/j.jlumin.2019.03.016.
[25] B. Warren XII, The structure of diopside, $CaMg(SiO_3)_2$., Z. Krist- Cryst, Mater 69 (1929) 168–193, https://doi.org/10.1524/zkri.1929.69.1.168.
[26] R.M. Thompson, R.T. Downs, The crystal structure of diopside at pressure to 10 GPa, Am. Mineral. 93 (2008) 177–186, https://doi.org/10.2138/am.2008.2684.
[27] R.D. Shannon, Revised effective ionic radii and systematic studies of interatomic distances in halides and chalcogenides, Acta Cryst. A. 32 (1976) 751–767, https://doi.org/10.1107/S0567739476001551.
[28] M. Akasaka, Y. Takasu, M. Handa, M. Nagashima, M. Hamada, T. Ejima, Distribution of Cr^{3+} between octahedral and tetrahedral sites in synthetic blue and green $(CaMgSi_2O_6)_{95}(CaCrAlSiO_6)_5$ diopsides, Min. Mag. 83 (2019) 497–505, https://doi.org/10.1180/mgm.2019.1.
[29] K. Ikeda, K. Yagi, Crystal-field spectra for blue and green diopsides synthesized in the join $CaMgSi_2O_6$-$CaCrAlSiO_6$, Contrib Mineral and Petr 81 (1982) 113–118, https://doi.org/10.1007/BF00372048.

[30] V.M. Khomenko, A.N. Platonov, Electronic absorption spectra of Cr^{3+} ions in natural clinopyroxenes, Phys. Chem. Miner. 11 (1985) 261–265, https://doi.org/10.1007/BF00307404.
[31] A.A. Setlur, A.M. Srivastava, On the relationship between emission color and Ce^{3+} concentration in garnet phosphors, Opt. Mater. 29 (2007) 1647–1652, https://doi.org/10.1016/j.optmat.2006.08.010.
[32] Z. Hao, J. Zhang, X. Zhang, Y. Luo, L. Zhang, H. Zhao, An intense blue-emitting phosphor for near-ultraviolet pumped white-light-emitting diodes: ce^{3+}-activated β-Ca_2SiO_4, J. Lumin. 152 (2014) 40–43, https://doi.org/10.1016/j.jlumin.2013.10.033.
[33] V. Bachmann, C. Ronda, A. Meijerink, Temperature Quenching of Yellow Ce^{3+} Luminescence in YAG:ce, Chem. Mater. 21 (2009) 2077–2084, https://doi.org/10.1021/cm8030768.
[34] L. Zhang, D. Wang, Z. Hao, X. Zhang, G. Pan, H. Wu, J. Zhang, Cr^{3+}-Doped Broadband NIR Garnet Phosphor with Enhanced Luminescence and its Application in NIR Spectroscopy, Adv. Opti. Mater. 7 (2019), 1900185, https://doi.org/10.1002/adom.201900185.
[35] T. Liu, H. Cai, N. Mao, Z. Song, Q. Liu, Efficient near-infrared pyroxene phosphor $LiInGe_2O_6$:cr^{3+} for NIR spectroscopy application, J. Am. Ceram .Soc. (2021), https://doi.org/10.1111/jace.17856 jace.17856.
[36] S. Kück, Laser-related spectroscopy of ion-doped crystals for tunable solid-state lasers, Appl. Phys. B. 72 (2001) 515–562, https://doi.org/10.1007/s003400100540.